Half-Metallic p-Type $LaAlO_3/EuTiO_3$ Heterointerface from Density-Functional Theory

Hai-Shuang Lu,[1] Tian-Yi Cai,[1] Sheng Ju,[1,*] and Chang-De Gong[2,3,†]

[1]*Department of Physics and Jiangsu Key Laboratory of Thin Films, Soochow University, Suzhou 215006, People's Republic of China*

[2]*Center for Statistical and Theoretical Condensed Matter Physics and Department of Physics, Zhejiang Normal University, Jinhua 321004, People's Republic of China*

[3]*National Laboratory of Solid State Microstructure and Department of Physics, Nanjing University, Nanjing 210093, People's Republic of China*

(Received 21 July 2014; revised manuscript received 4 December 2014; published 31 March 2015)

The two-dimensional electron gas (2DEG) observed at the $LaAlO_3/SrTiO_3$ heterointerface has attracted intense research interest in recent years. The high mobility, electric tunability, and giant persistent photoconductivity suggest its potential for electronic and photonic applications. The lack of a p-type counterpart as well as a highly spin-polarized carrier in the $LaAlO_3/SrTiO_3$ system, however, restricts its widespread application, since both multiple carriers and high spin polarization are very desirable for electronic devices. Here, we report a system of $LaAlO_3/EuTiO_3$ digital heterostructures that may overcome these limitations. Results from first-principles calculations reveal that the 2DEG in the n-type $LaAlO_3/EuTiO_3$ is a normal ferromagnet. The p-type two-dimensional hole gas, on the other hand, is a 100% spin-polarized half-metal. For digital heterostructures with alternating n-type and p-type interfaces, a magnetic-field-driven insulator-to-metal transition, together with spatially separated electrons and holes, can be realized by tuning the intrinsic polar field. At low temperatures, the spin-polarized electron-hole pairs may result in spin-triplet exciton condensation, which provides an experimentally accessible system for achieving the theoretically proposed dissipationless spin transport. Our findings open a path for exploring spintronics at the heterointerface of transition-metal oxides.

DOI: 10.1103/PhysRevApplied.3.034011

I. INTRODUCTION

Electric currents can be completely spin polarized in a class of materials known as half-metals, as a result of the coexistence of the metallic nature for electrons with one spin orientation and the insulating nature for electrons with the other [1]. In view of their potential applications in spin-based electronic devices [2–4], a substantial effort has been made to search for new half-metallic materials [5–11]. Carrier doping in transition-metal oxides is an effective avenue towards a highly spin-polarized state. An example is doped manganites, which develop a double-exchange-driven half-metallicity [12,13]. However, the randomly distributed dopants could act as scattering centers, resulting in a substantially decreased spin polarization which restricts the highly spin-polarized state in a narrow region of the phase diagram [14,15].

A charge transfer via the polar catastrophe mechanism across a heterointerface is an alternative way to realize carrier doping which can proceed in a controllable manner. A well-known example is the two-dimensional electron gas (2DEG) revealed at the $LaAlO_3/SrTiO_3$ heterointerface [16], which exhibits a weak ferromagnetism and even superconductivity at low temperatures [17,18]. To enhance the magnetism in these systems, ferromagnetic (FM) semiconductor EuO with the $4f$ element was first introduced in the n-type $LaAlO_3/EuO$ heterointerface [19,20]. Later, $3d$ materials [either the nonmagnetic FeS_2 [21] or the antiferromagnetic (AFM) $SrMnO_3$ [22]] have been proposed to replace $SrTiO_3$. However, all these structures are n type. A p-type counterpart, i.e., a two-dimensional hole gas (2DHG), is still not available.

To create highly spin-polarized 2DEG and 2DHG, we propose an alternative design strategy by assigning the electron and hole degrees of freedom at different atomic sites. Perovskite $EuTiO_3$ with unusual f-d exchange coupling could be an interesting candidate [23–34]. Pioneering experiments on La-doped $EuTiO_3$ show a G-type AFM-to-FM phase transition upon electron doping [35,36]. Furthermore, the existence of both Eu^{2+} and Eu^{3+} suggests that, besides realizing the electron doping via the $Ti^{4+} \rightarrow Ti^{3+}$ transition, hole doping via $Eu^{2+} \rightarrow Eu^{3+}$ might also be experimentally achievable in this quantum paraelectric material [37].

Here we demonstrate that, by designing polar-nonpolar digital heterostructures of $LaAlO_3/EuTiO_3$, carrier doping via a charge transfer across the heterointerface can be realized and will give rise to several spintronic properties, including a half-metallic electronic state, a magnetic-ordering-driven insulator-to-metal transition with a colossal

*jusheng@suda.edu.cn
†cdgongsc@nju.edu.cn

magnetoresistive effect, and a spin-triplet exciton formation which shows a dissipationless spin-transport property. These findings not only are of great scientific interest but may also open a path to explore spintronics at the heterointerface of transition-metal oxides.

II. STRUCTURE AND COMPUTATIONAL DETAILS

In order to study the electronic reconstruction at the $LaAlO_3/EuTiO_3$ heterointerfaces, as demonstrated in Fig. 1, we consider two kinds of heterointerface: an *n*-type, i.e., $(LaO)^+/(TiO_2)^0$, interface, and a *p*-type, i.e., $(AlO_2)^-/(EuO)^0$, interface. The combination of these interfaces may give rise to *nn*-type superlattices consisting of only *n*-type heterointerfaces, *pp*-type superlattices, and *np*-type superlattices. As shown in the studies of the $LaAlO_3/SrTiO_3$ heterointerfaces [38–41], these three kinds of superlattice structure can provide a comprehensive picture of the electronic reconstruction at the polar-nonpolar heterointerfaces. The first two kinds of superlattice are symmetric structures with an additional $(LaO)^+$ layer or $(AlO_2)^-$ layer to form the *nn*-type heterostructure or the *pp*-type heterostructure, respectively. These structures correspond to the thick $LaAlO_3$ limit, which guarantees 0.5 electrons (or 0.5 holes) per cell being transferred

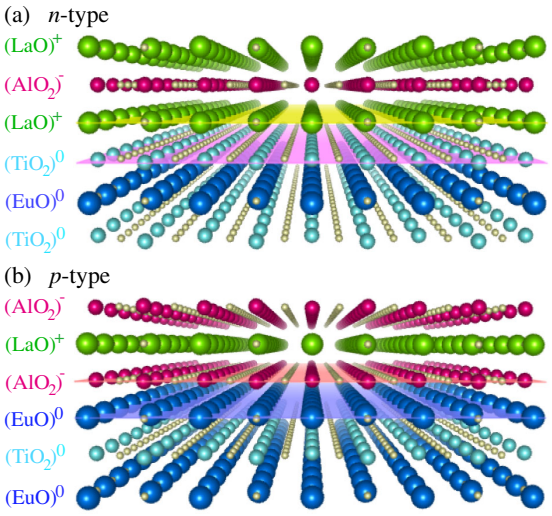

FIG. 1. $LaAlO_3/EuTiO_3$ heterointerfaces. (a) *n*-type $(LaO)^+/(TiO_2)^0$. (b) *p*-type $(AlO_2)^-/(EuO)^0$. Generally, in the ionic limit, $EuTiO_3$ is composed of charge-neutral atomic layers of $(EuO)^0$ and $(TiO_2)^0$, while $LaAlO_3$ consists of positively charged $(LaO)^+$ and negatively charged $(AlO_2)^-$ atomic layers. When $LaAlO_3$ is grown epitaxially on the $EuTiO_3$ substrate, an intrinsic electric field directed from $(LaO)^+$ to $(AlO_2)^-$ is formed through $LaAlO_3$, resulting in a potential difference which will diverge with increasing $LaAlO_3$ thickness. To offset the diverging potential difference, an electronic reconstruction is expected, where each $(LaO)^+/(TiO_2)^0$ needs 1/2 electron and each $(AlO_2)^-/(EuO)^0$ needs 1/2 hole.

across the interface [41]. For the *np*-type superlattice structure, the intrinsic polar field gives rise to a zigzag potential which will ultimately lead to an insulator-to-metal transition when the system is thick enough [40]. We use *N*-*M* to label our digital heterostructures, where *N* is the total number of perovskite units and *M* indicates the number of TiO_2 layers.

Our *ab initio* calculations are performed by using the accurate full potential projector-augmented-wave (PAW) method [42] as implemented in the Vienna *ab initio* simulation package (VASP) [43]. The generalized gradient approximation (GGA) in the form proposed by Perdew, Burke, and Ernzerhof is used [44]. The on-site Coulomb correlation is included within the GGA + *U* approach with an effective Hubbard $U = 4$ eV for the Eu $4f$ orbitals [45,46]. Within the GGA + *U*, a kind of magnetic ordering is assumed. However, when the system evolves into the paramagnetic state (above the Néel temperature or Curie temperature), a method which could describe the fluctuating moments properly should be used. A large plane-wave cutoff of 600 eV is used throughout the calculations, and the convergence criteria for the energy is 10^{-6} eV. The PAW potentials are used to describe the electron-ion interaction, with 17 valence electrons for Eu ($5s^25p^64f^76s^2$), 12 for Ti ($3s^23p^63d^24s^2$), nine for La ($5p^65d^16s^2$), three for Al ($3s^23p^1$), and six for O ($2s^22p^4$). A $12 \times 12 \times (4/N)$ (*N* is the total number of ABO_3 perovskite units) Monkhorst-Pack *k*-point mesh centered at the Γ point is used. In our calculations, the in-plane lattice constant is fixed as 3.946 Å; this value is the GGA-optimized lattice constant for the substrate $SrTiO_3$. Ions are relaxed until the Hellman-Feynman forces are less than 1 meV/Å and the *c* axis is optimized. For the electronic density-of-states calculations, a much denser *k* mesh of $24 \times 24 \times (8/N)$ is used for the Brillouin-zone integrations. We use an in-plane $\sqrt{2}a \times \sqrt{2}a$ geometry (where *a* is the in-plane lattice constant of the perovskite ABO_3). Preliminary calculations of bulk $EuTiO_3$ of either fully optimized structure or bulk strained on the $SrTiO_3$ substrate show that the G-type AFM ordering is the ground state [46]. This result is in good agreement with the experimental observation and previous *ab initio* results [26,30,31]. Additional calculations with the $a^0a^0c^-$ rotation (i.e., space group $I4/mcm$ no. 140) [30] included do not change the main results. The energy gain for FM ordering through the carrier doping in these digital heterostructures is much larger than that arising from the spin-lattice coupling [30,31].

III. RESULTS AND DISCUSSION

A. *nn*-type and *pp*-type heterostructures

We first focus on two types of digital heterostructure which are composed of *n*-type or *p*-type interfaces solely. Clearly, the FM ordering is energetically favorable in both situations [46]. With an increasing thickness of $EuTiO_3$, the

energy difference between the G-type AFM and the FM orderings decreases. In addition, the calculated electronic structures indicate that the n-type interfaces are normal ferromagnets and the p-type ones are half-metals [46].

To show the differences between the n-type and p-type digital heterostructures, an nn-type 4-3 and a pp-type 4-1 digital heterostructure are demonstrated in Fig. 2; both structures have two neighboring EuO atomic layers. For the n-type system [also shown in Fig. 3(a)], the occupied conduction bands are mostly composed of Ti t_{2g} states, and the lowest two bands are well localized on the first Ti (Ti1) layers with an xy symmetry due to the much lower interface potential and greater hopping integrals along the planar directions. This result can also be seen by plotting the real space orbitals of each band [see Fig. 3(b)]. From left to right, they are of xy, xy, xz/yz, xz/yz, and xy characteristics for the up-spin channel and of xy, xy, xy, xz/yz, and xz/yz characteristics for the down-spin channel. Because of the small supercell used in our calculations, the Ti1 xy bands belonging to the two interfaces mix together with a sizable splitting near the Γ point. Above these bands, there are the yz/xz bands and the xy bands located on the second Ti (Ti2) layer; the former consist of a linear combination of states on all the Ti layers and have a weak dispersion along the planar directions. Different from the carriers in the n-type $LaAlO_3/SrTiO_3$ heterostructure [39], all xy orbitals show a strong 2D characteristic. In particular, the xy orbital

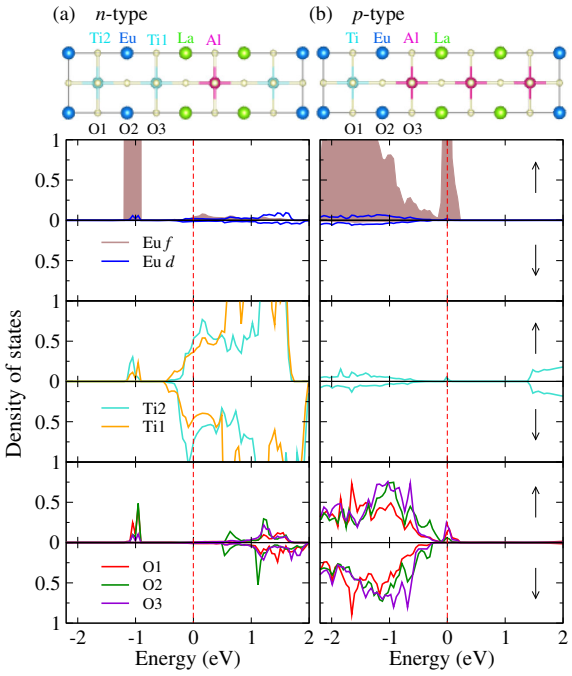

FIG. 2. (a) Upper panel: Illustration of the symmetric nn-type 4-3 $LaAlO_3/EuTiO_3$ digital heterostructure. Lower panel: Partial density of states in nn-type 4-3. (b) Upper panel: Illustration of the symmetric pp-type 4-1 $LaAlO_3/EuTiO_3$ digital heterostructure. Lower panel: Partial density of states in pp-type 4-1. The Fermi level is indicated at energy zero with a dashed line.

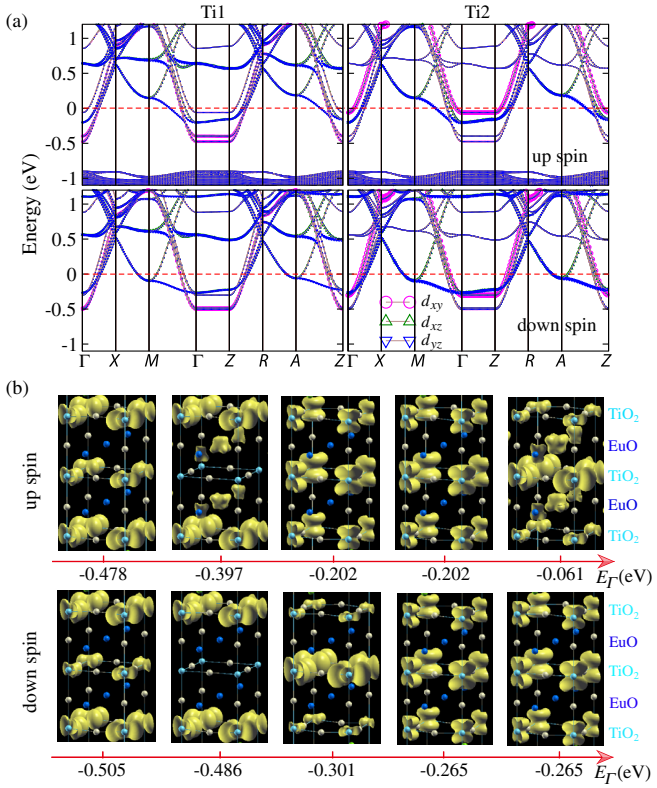

FIG. 3. (a) Orbital-resolved band structure of nn-type 4-3. The Fermi energy is set to zero. (b) The squared wave function of states corresponding to the eigenvalues (Γ point) labeled below.

at the inner Ti shows a strong exchange splitting, which can be localized by disorder. The xz/yz states, on the other hand, have a heavy mass along the planar directions. However, their spreading through all the Ti sites will make them active in the transport. Our result on the FM 2DEG at the n-type heterointerface is in good agreement with recent experimental findings, where ferromagnetically ordered Eu^{2+} spins and a finite metallic conductivity are identified in the heterostructures of $LaAlO_3/EuTiO_3/SrTiO_3$ when the thickness of the $LaAlO_3$ layer is greater than three unit cells [47]. The experimentally observed reduced magnetic moment of around $3.5\mu_B$ is thought to be related to the appearance of Eu^{3+} during the deposition of these ultrathin films in an oxidizing atmosphere [47]. In addition, the existence of oxygen vacancies could have a complicated influence on the magnetic and transport properties at the heterointerfaces of transition-metal oxides. For $EuTiO_3$, electron doping via the oxygen vacancies may mediate a FM ordering of Eu spins.

On the other hand, for the p-type system, as demonstrated in Fig. 4(a), the Fermi level crosses only the top of valence bands in the up-spin channel, showing a half-metallic behavior. The unoccupied Ti states in the bulk $EuTiO_3$ are still empty, and the density of states at the Fermi level arises mainly from the Eu $4f$ states slightly mixed with the O $2p$ states. As shown in Fig. 4(b), the

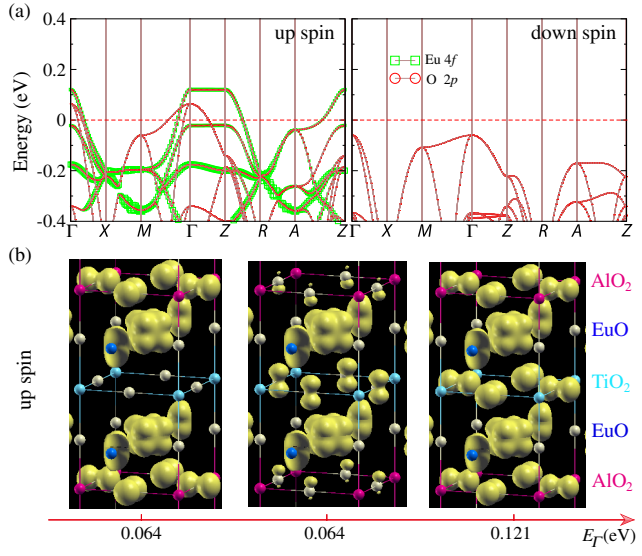

FIG. 4. (a) Orbital-resolved band structure of pp-type 4-1. The Fermi energy is set to zero. (b) The squared wave function of states corresponding to the eigenvalues (Γ point and up-spin channel) labeled below.

unoccupied states (holes) are found to be extended to the whole structure via the oxygen $2p$ states located at each layer. A local magnetic moment of $6.5\mu_B$ is found at the Eu site, which is smaller than the $7\mu_B$ found in bulk $EuTiO_3$, indicating the presence of holes in the Eu $4f$ states. By analyzing the band dispersion and the real space orbitals, we find that the holes centered around the Γ point are well localized at the interfacial Eu layers with f_{xyz} symmetry. The oxygen $2p$ states lie below the Eu f_{xyz} state. In contrast to the oxygen-vacancy-induced p-type half-metallic electronic state in CaO [48] and $KTaO_3/SrTiO_3$ [49], the spin-polarized holes in $LaAlO_3/EuTiO_3$ are derived from the Eu $4f$ orbitals, which possess robust and strong local magnetic moments compared with the oxygen $2p$ orbitals. Furthermore, fully spin-polarized p-type carriers are of technological importance. Current spintronic devices (e.g., the giant magnetoresistance head in hard disks or the tunneling magnetoresistance junction in the nonvolatile memory) are based on FM metals [2–4]. The availability of two kinds of 100% spin-polarized carrier will provide a solid foundation for next-generation spintronic devices. The basic unit of p-n junctions, on which most conventional semiconductor devices are based, could be explored further for functionalities with the spin degrees of freedom included.

It should be mentioned that, energetically, bulk $EuTiO_3$ is near the phase boundary between the G-type AFM and the FM orderings, where the AFM superexchange via the Ti $3d$ orbitals competes with FM indirect exchange through the Eu $5d$ orbitals [32]. For bulk $EuTiO_3$, the G-type AFM ordering is the ground state [23,26]. If the relative strength of the AFM and FM interactions is modified by external perturbations such as epitaxial strain [26,27,31], an external electric field [33], or electron doping [35,36,47], the FM ordering could become the ground state.

This result motivates us to investigate the relationship between the charge transfer via electrostatic doping and the FM ordering in these heterostructures. In Fig. 5(b), we show the electronic density of states projected onto atomic planes in $EuTiO_3$ and $LaAlO_3$. These results indicate that most of the doped electrons reside in the TiO_2 layer while holes favor the EuO layer. Ionic relaxations allow for additional ionic compensation of the interface dipole, resulting in a buckling structure with the oxygen atoms moving towards the interface and the cations away from it [see Fig. 5(c)]. The largest cation-anion displacement of about 0.120 Å is revealed at interfacial TiO_2 and EuO

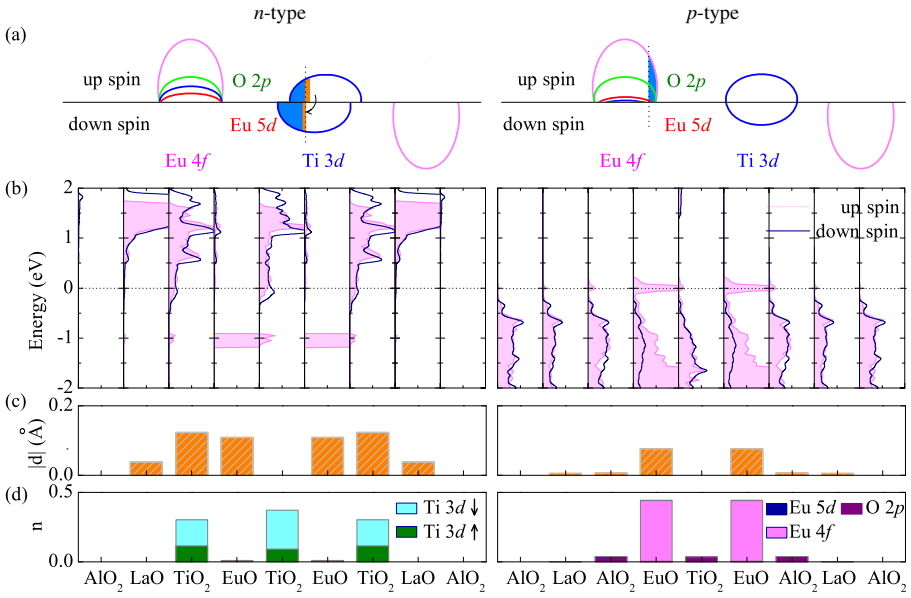

FIG. 5. The origin of half-metallicity. (a) Band diagram at $LaAlO_3/EuTiO_3$ heterointerfaces. (b) Layer-projected density of states of nn-type 4-3 and pp-type 4-1. (c) The anion-cation splitting for EuO and TiO_2 planes in $EuTiO_3$ and LaO and AlO_2 planes in $LaAlO_3$. Here, $d = z_{\text{cation}}$-z_{anion}. (d) The sheet carrier number of each layer.

layers in the nn-type 4-3 structure. For the pp-type 4-1 structure, the interfacial EuO layer shows the largest displacement of 0.075 Å.

The "sheet carrier number" is defined as the sum of all conducting electrons in the Ti $3d$ states (both spin channels) and the Eu $4f$ and $5d$ states for the nn-type 4-3 structure and all conducting holes in the Eu $4f$ and $5d$ states and the O $2p$ state for the pp-type 4-1 structure. For the symmetric nn-type and pp-type digital heterostructures studied here, one hole or one electron per supercell should exist compared with the nominal ionic charges [41]. For the nn-type system, we find that about 0.66 electrons reside in the down-spin channel and 0.32 electrons in the up-spin channel. In comparison, for the pp-type 4-1 structure, about 88% of the doped holes can be characterized as the Eu $4f$ states. Obviously, either additional electrons in the originally empty Ti conduction band or holes in the fully occupied Eu valence band will reduce the AFM exchange interaction between the Eu $4f$ electrons. Therefore, the electrostatic doping breaks the delicate balance between the magnetic interactions in $EuTiO_3$ and drives a magnetic transition from the G-type AFM ordering to the FM ground state in $LaAlO_3/EuTiO_3$ digital heterostructures.

However, one question remains unanswered: Why does the n-type $LaAlO_3/EuTiO_3$ heterointerface exhibit normal ferromagnetism while the p-type structure is half-metallic? Here, the hybridization between the localized $4f$ (Eu) state and itinerant $3d$ (Ti) electrons is the key to understanding the fundamental mechanism. A schematic illustration of the band diagram for the FM state is shown in Fig. 5(a). If the $3d$ (Ti)–$4f$ (Eu) hybridization is switched on in the FM ordering of the Eu $4f$ orbitals, the majority spin Ti $3d$ bands will shift toward higher energy due to the d-f hybridization, while the minority spin Ti $3d$ bands make an opposite shift. An energy gain is therefore obtained by transferring the electrons from the Ti $3d$ majority spin to the minority spin channel. Obviously, the essential ingredient in this mechanism is the energy gain produced by a negative spin polarization of the Ti $3d$ states, which agrees with our first-principles calculations. This observation also provides a deeper understanding of the recent experimental findings where the filling of the Ti $3d$ states is expected to account for the observed ferromagnetism at the n-type heterointerface of $LaAlO_3/EuTiO_3/SrTiO_3$ structure [47]. Further direct measurement of the spin polarization using spin-polarized photoemission or the local magnetic moments would help to verify our theoretical understanding. For the p-type heterostructure, the doped holes mostly go to the relatively localized Eu $4f$ states. The high density of states at the Fermi level $D(E_F)$ provides an excellent mechanism to realize Stoner ferromagnetism, and the large exchange splitting of the Eu $4f$ orbitals makes hole-doped $EuTiO_3$ half-metallic. It should also be pointed out that the energy differences between the FM ordering and the AFM states in these superlattices structures are much larger than those of bulk $EuTiO_3$ [46], indicating a possible enhancement of the FM transition temperatures.

B. *np*-type heterostructures

Next, we show the electronic and magnetic properties of the stoichiometric np-type $LaAlO_3/EuTiO_3$ digital heterostructures, where, as shown in Fig. 6, the band gap can be effectively tuned via the inherent polar field [40]. With the increase of the thickness of the $LaAlO_3$ polar layer, the band gap of the np-type $LaAlO_3/EuTiO_3$ digital heterostructures is gradually closed (see Fig. 7). For the single $EuTiO_3$ layer digital heterostructures, the AFM ordering is still energetically favorable [46]. However, in the FM state, conduction bands of the down-spin channel shift towards the Fermi level, and a magnetic-field-driven insulator-to-metal transition accompanied with a colossal magnetoresistive effect is therefore expected. When the thickness of the $EuTiO_3$ layer increases further, the FM ordering becomes the ground state and the systems are metallic [46].

In digital heterostructures with alternating n-type and p-type interfaces (e.g., $LaAlO_3/SrTiO_3$ np-type heterostructures [40,50]), the inherent zigzagging electrostatic potential will lead to a spatial separation between electrons and holes. In addition, the strong Coulomb interaction, as that in the conventional electron-hole bilayer system, will not only induce functionalities [51] but may also drive these electron-hole pairs into a superfluid state at low temperatures [52–54]. In $LaAlO_3/EuTiO_3$ digital heterostructures as we discussed above, both 2DEG at the n-type interface and 2DHG at the p-type side should be spin polarized. Surprisingly, in the thinnest limit of $EuTiO_3$ as shown in Fig. 8(a), the Ti $3d$ states are also completely spin polarized in the FM state. The up-spin carriers are electronlike, while the down-spin carriers are holelike. It is anticipated that due to the small distance between these positively and negatively charged carriers, as shown in Fig. 8(c), they may attract each other and form electron-hole pairs via strong Coulomb interaction. In addition, the filled Ti $3d$ (electron) states locate below the Eu $4f$ (hole) states, therefore effectively preventing an electron-hole recombination [see Fig. 8(b)]. With this unique band structure, the condensation of spin-triplet exciton states in $LaAlO_3/EuTiO_3$ [see

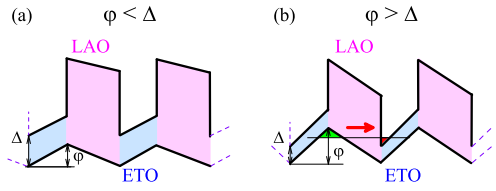

FIG. 6. Illustration of the band diagram of np-type $LaAlO_3/EuTiO_3$ (LAO/ETO) digital heterostructures. Depending on the relative strength between the polar field and band gap, the system could be insulating for $\varphi < \Delta$ (a) or metallic for $\varphi > \Delta$ (b).

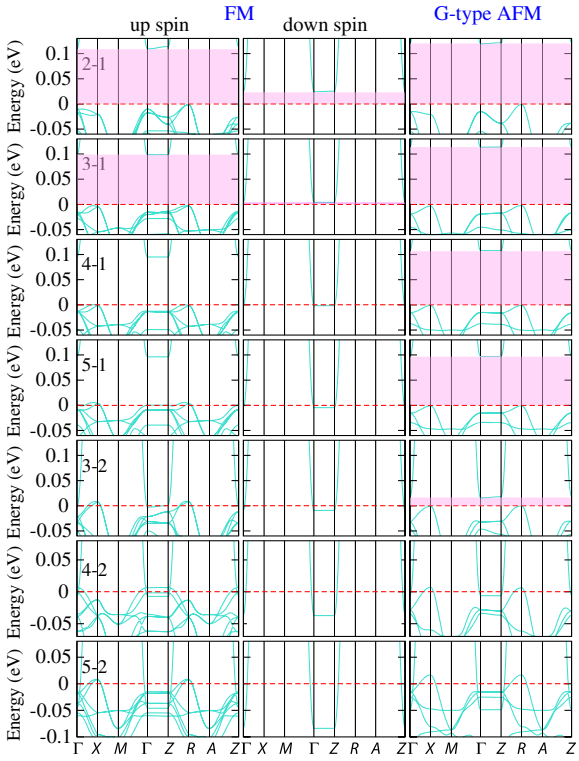

FIG. 7. Evolution of the electronic band structure of np-type $LaAlO_3/EuTiO_3$ digital heterostructures. With increasing thickness of the polar layer $LaAlO_3$, the band gap is gradually closed, and an insulator-to-metal transition is expected when $LaAlO_3/EuTiO_3$ is thick enough, consistent with the scenario of polar-catastrophe-driven charge transfer at the np-type digital heterostructures [40]. In addition, a FM-ordering-driven insulator-to-metal transition is also observed when the gap in the G-type AFM state is small. In all figures, the Fermi energy is set to zero and indicated with a dashed line.

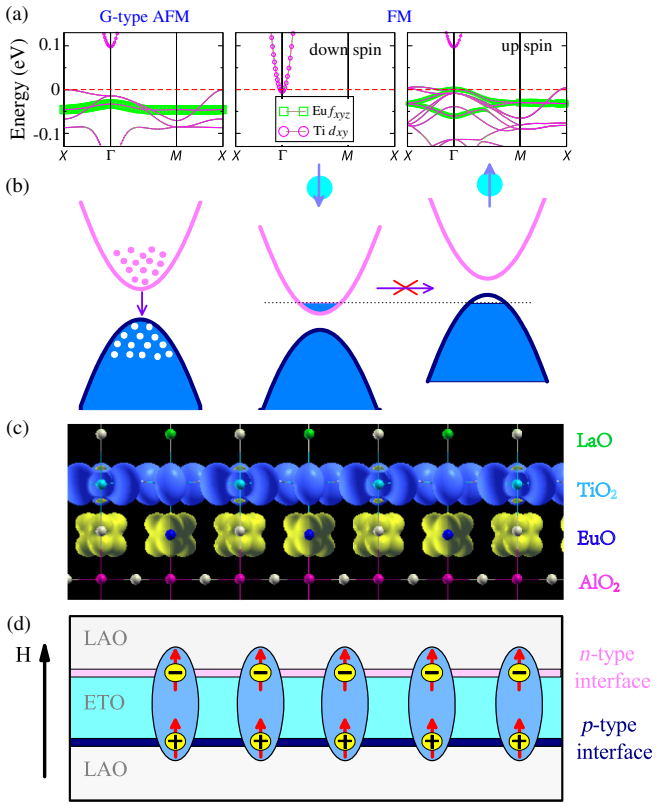

FIG. 8. (a) Electronic band structure of np-type 5-1. (b) Illustration of conventional electron-hole excitation in a semiconductor (left) and its current picture in np-type 5-1 within a FM state. (c) The squared wave function of states corresponding to the eigenvalues of the conduction band minimum (Γ point and down-spin channel) and the valence band maximum (Γ point and up-spin channel) in the FM state. (d) Illustration of the spin-triplet exciton.

Fig. 8(d)] could provide a real material system towards dissipationless spin transport, which is proposed prototypically in graphene systems under strong magnetic fields [55–57]. Here, the energy difference between the FM state and the AFM ground state is 0.81 meV, which could be experimentally accessible. Further experiments on the p-type $LaAlO_3/EuTiO_3$ heterointerfaces [47] are highly expected.

Finally, it should be pointed out that oxide heterostructures provide many systems with unusual magnetic properties and attract great interest from researchers in condensed matter physics and materials science [58–63]. In addition, heterostructures show promising properties for spin manipulation [64,65]. The observations of fully spin-polarized multiple carriers will not only broaden such interest from single-particle phenomena to many-body effects but also show potential applications in spintronics devices. $LaAlO_3/EuTiO_3$ digital heterostructure, as we demonstrate in this paper, may provide an exciting example towards realizing the concept "the interface is the device" [66].

IV. SUMMARY

In summary, by designing a polar-nonpolar digital heterostructure of $LaAlO_3/EuTiO_3$, we demonstrate systems with two-dimensional half-metallic electronic states and fully spin-polarized carriers. For the p-type heterointerface, the half-metallic state arises from a large exchange splitting of the strongly localized Eu $4f$ orbitals and the high density of states at the Fermi level even with low carrier-doping concentrations. On the other hand, for the n-type heterointerface, the bottom of Ti $3d$ conduction bands is partially occupied and possesses a negative spin polarization driven by the strong hybridization between the localized Eu $4f$ states and the itinerant Ti $3d$ orbitals. Surprisingly, when the n-type and the p-type heterointerfaces are brought together, a magnetic-field-driven insulator-to-metal transition and a colossal magnetoresistive effect are found. In addition, the unique band structure with a spatial separation between the fully spin-polarized electron pocket and the hole pocket could provide a real material system for realizing spin-triplet exciton

condensation and ultimately dissipationless spin transport. Our results show that the $LaAlO_3/EuTiO_3$ digital heterostructures display unique and unusual electronic and magnetic properties which may be useful for spintronic applications.

ACKNOWLEDGMENTS

This work was supported by the National Basic Research Program of China (973 Program 2013CB934400 and 2014CB920900), the National Natural Science Foundation of China under Grants No. 11104193 and No. 11374220, and the Project Funded by the Priority Academic Program Development of Jiangsu Higher Education Institutions.

[1] R. A. de Groot, F. M. Mueller, P. G. van Engen, and K. H. J. Buschow, New Class of Materials: Half-Metallic Ferromagnets, Phys. Rev. Lett. **50**, 2024 (1983).
[2] I. Žutić, J. Fabian, and S. Das Sarma, Spintronics: Fundamentals and applications, Rev. Mod. Phys. **76**, 323 (2004).
[3] A. Fert, Nobel lecture: Origin, development, and future of spintronics, Rev. Mod. Phys. **80**, 1517 (2008).
[4] P. A. Grünberg, Nobel lecture: From spin waves to giant magnetoresistance and beyond, Rev. Mod. Phys. **80**, 1531 (2008).
[5] W. E. Pickett and J. S. Moodera, Half-metallic magnets, Phys. Today **54**, No. 5, 39 (2001).
[6] M. I. Katsnelson, V. Yu. Irkhin, L. Chioncel, A. I. Lichtenstein, and R. A. de Groot, Half-metallic ferromagnets: From band structure to many-body effects, Rev. Mod. Phys. **80**, 315 (2008).
[7] Y. W. Son, M. L. Cohen, and S. G. Louie, Half-metallic graphene nanoribbons, Nature (London) **444**, 347 (2006).
[8] X. Hu, Half-metallic antiferromagnet as a prospective material for spintronics, Adv. Mater. **24**, 294 (2012).
[9] T. Jungwirth, J. Sinova, J. Mašek, J. Kučera, and A. H. MacDonald, Theory of ferromagnetic (III,Mn)V semiconductors, Rev. Mod. Phys. **78**, 809 (2006).
[10] K. Sato *et al.*, First-principles theory of dilute magnetic semiconductors, Rev. Mod. Phys. **82**, 1633 (2010).
[11] T. Dietl and H. Ohno, Dilute ferromagnetic semiconductors: Physics and spintronic structures, Rev. Mod. Phys. **86**, 187 (2014).
[12] J. M. D. Coey, M. Viret, and S. von Molnár, Mixed valence manganites, Adv. Phys. **48**, 167 (1999).
[13] M. B. Salamon and M. Jaime, The physics of manganites: Structure and transport, Rev. Mod. Phys. **73**, 583 (2001).
[14] E. Dagotto, T. Hotta, and A. Moreo, Colossal magnetoresistant materials: The key role of phase separation, Phys. Rep. **344**, 1 (2001).
[15] Y. Tokura, Critical features of colossal magnetoresistive manganites, Rep. Prog. Phys. **69**, 797 (2006).
[16] J. Mannhart, D. H. A. Blank, H. Y. Hwang, A. J. Millis, and J. M. Triscone, Two-dimensional electron gases at oxide interfaces, MRS Bull. **33**, 1027 (2008).
[17] K. Michaeli, A. C. Potter, and P. A. Lee, Superconducting and Ferromagnetic Phases in $SrTiO_3/LaAlO_3$ Oxide Interface Structures: Possibility of Finite Momentum Pairing, Phys. Rev. Lett. **108**, 117003 (2012).
[18] G. Chen and L. Balents, Ferromagnetism in Itinerant Two-Dimensional t_{2g} Systems, Phys. Rev. Lett. **110**, 206401 (2013).
[19] Y. Wang, M. K. Niranjan, J. D. Burton, J. M. An, K. D. Belashchenko, and E. Y. Tsymbal, Prediction of a spin-polarized two-dimensional electron gas at the $LaAlO_3/EuO(001)$ interface, Phys. Rev. B **79**, 212408 (2009).
[20] J. Lee, N. Sai, and A. A. Demkov, Spin-polarized two-dimensional electron gas through electrostatic doping in $LaAlO_3/EuO$ heterostructures, Phys. Rev. B **82**, 235305 (2010).
[21] J. D. Burton and E. Y. Tsymbal, Highly Spin-Polarized Conducting State at the Interface between Nonmagnetic Band Insulators: $LaAlO_3/FeS_2$ (001), Phys. Rev. Lett. **107**, 166601 (2011).
[22] F. Hou, T. Y. Cai, S. Ju, and M. R. Shen, Half-metallic ferromagnetism via the interface electronic reconstruction in $LaAlO_3/SrMnO_3$ nanosheet superlattices, ACS Nano **6**, 8552 (2012).
[23] C. L. Chien, S. DeBenedetti, and F. De S. Barros, Magnetic properties of $EuTiO_3$, Eu_2TiO_4, and $Eu_3Ti_2O_7$, Phys. Rev. B **10**, 3913 (1974).
[24] T. Katsufuji and H. Takagi, Coupling between magnetism and dielectric properties in quantum paraelectric $EuTiO_3$, Phys. Rev. B **64**, 054415 (2001).
[25] H. Wu, Q. Jiang, and W. Z. Shen, Coupling between the magnetism and dielectric properties in $Eu_{1-x}Ba_xTiO_3$, Phys. Rev. B **69**, 014104 (2004).
[26] C. J. Fennie and K. M. Rabe, Magnetic and Electric Phase Control in Epitaxial $EuTiO_3$ from First Principles, Phys. Rev. Lett. **97**, 267602 (2006).
[27] J. H. Lee *et al.*, A strong ferroelectric ferromagnet created by means of spin-lattice coupling, Nature (London) **466**, 954 (2010).
[28] H. Akamatsu, Y. Kumagai, F. Oba, K. Fujita, H. Murakami, K. Tanaka, and I. Tanaka, Antiferromagnetic superexchange via 3d states of titanium in $EuTiO_3$ as seen from hybrid Hartree-Fock density functional calculations, Phys. Rev. B **83**, 214421 (2011).
[29] J. L. Bettis, M. H. Whangbo, J. Köhler, A. Bussmann-Holder, and A. R. Bishop, Lattice dynamical analogies and differences between $SrTiO_3$ and $EuTiO_3$ revealed by phonon-dispersion relations and double-well potentials, Phys. Rev. B **84**, 184114 (2011).
[30] K. Z. Rushchanskii, N. A. Spaldin, and M. Lezaic, First-principles prediction of oxygen octahedral rotations in perovskite-structure $EuTiO_3$, Phys. Rev. B **85**, 104109 (2012).
[31] Y. Yang, W. Ren, D. Wang, and L. Bellaiche, Understanding and Revisiting Properties of $EuTiO_3$ Bulk Material and Films from First Principles, Phys. Rev. Lett. **109**, 267602 (2012).
[32] T. Birol and C. J. Fennie, Origin of giant spin-lattice coupling and the suppression of ferroelectricity in $EuTiO_3$ from first principles, Phys. Rev. B **88**, 094103 (2013).

[33] P. J. Ryan *et al.*, Reversible control of magnetic interactions by electric field in a single-phase material, Nat. Commun. **4**, 1334 (2013).

[34] Y. Geng, J. H. Lee, D. G. Schlom, J. W. Freeland, and W. Wu, Magnetic inhomogeneity in a multiferroic $EuTiO_3$ thin film, Phys. Rev. B **87**, 121109(R) (2013).

[35] T. Katsufuji and Y. Tokura, Transport and magnetic properties of a ferromagnetic metal: $Eu_{1-x}R_xTiO_3$, Phys. Rev. B **60**, R15021(R) (1999).

[36] K. S. Takahashi, M. Onoda, M. Kawasaki, N. Nagaosa, and Y. Tokura, Control of the Anomalous Hall Effect by Doping in $Eu_{1-x}La_xTiO_3$ Thin Films, Phys. Rev. Lett. **103**, 057204 (2009).

[37] Do Le Binh, B. J. Ruck, F. Natali, H. Warring, H. J. Trodahl, E.-M. Anton, C. Meyer, L. Ranno, F. Wilhelm, and A. Rogalev, Europium Nitride: A Novel Diluted Magnetic Semiconductor, Phys. Rev. Lett. **111**, 167206 (2013).

[38] M. S. Park, S. H. Rhim, and A. J. Freeman, Charge compensation and mixed valency in $LaAlO_3/SrTiO_3$ heterointerfaces studied by the FLAPW method, Phys. Rev. B **74**, 205416 (2006).

[39] Z. S. Popović, S. Satpathy, and R. M. Martin, Origin of the Two-Dimensional Electron Gas Carrier Density at the $LaAlO_3$ on $SrTiO_3$ Interface, Phys. Rev. Lett. **101**, 256801 (2008).

[40] N. C. Bristowe, E. Artacho, and P. B. Littlewood, Oxide superlattices with alternating p and n interfaces, Phys. Rev. B **80**, 045425 (2009).

[41] H. H. Chen, A. M. Kolpak, and S. Ismail-Beigi, Electronic and magnetic properties of $SrTiO_3/LaAlO_3$ interfaces from first principles, Adv. Mater. **22**, 2881 (2010).

[42] P. E. Blöchl, Projector augmented-wave method, Phys. Rev. B **50**, 17953 (1994).

[43] G. Kresse and J. Furthmüller, Efficiency of ab-initio total energy calculations for metals and semiconductors using a plane-wave basis set, Comput. Mater. Sci. **6**, 15 (1996).

[44] J. P. Perdew, K. Burke, and M. Ernzerhof, Generalized Gradient Approximation Made Simple, Phys. Rev. Lett. **77**, 3865 (1996).

[45] S. L. Dudarev, G. A. Botton, S. Y. Savrasov, C. J. Humphreys, and A. P. Sutton, Electron-energy-loss spectra and the structural stability of nickel oxide: An LSDA + U study, Phys. Rev. B **57**, 1505 (1998).

[46] See Supplemental Material athttp://link.aps.org/supplemental/10.1103/PhysRevApplied.3.034011 for total energies, lattice constants, density of states, and calculations of Hubbard U dependence.

[47] G. M. De Luca *et al.*, Transport properties of a quasi-two-dimensional electron system formed in $LaAlO_3/EuTiO_3/SrTiO_3$ heterostructures, Phys. Rev. B **89**, 224413 (2014).

[48] I. S. Elfimov, S. Yunoki, and G. A. Sawatzky, Possible Path to a New Class of Ferromagnetic and Half-Metallic Ferromagnetic Materials, Phys. Rev. Lett. **89**, 216403 (2002).

[49] R. Oja *et al.*, d^0 Ferromagnetic Interface between Nonmagnetic Perovskites, Phys. Rev. Lett. **109**, 127207 (2012).

[50] R. Pentcheva *et al.*, Parallel Electron-Hole Bilayer Conductivity from Electronic Interface Reconstruction, Phys. Rev. Lett. **104**, 166804 (2010).

[51] K. Wu, L. Rademaker, and J. Zaanen, Bilayer Excitons in Two-Dimensional Nanostructures for Greatly Enhanced Thermoelectric Efficiency, Phys. Rev. Applied **2**, 054013 (2014).

[52] J. P. Eisenstein and A. H. MacDonald, Bose-Einstein condensation of excitions in bilayer electron systems, Nature (London) **432**, 691 (2004).

[53] A. V. Balatsky, Y. N. Joglekar, and P. B. Littlewood, Dipolar Superfluidity in Electron-Hole Bilayer Systems, Phys. Rev. Lett. **93**, 266801 (2004).

[54] J.-J. Su and A. H. MacDonald, How to make a bilayer exciton condensate flow, Nat. Phys. **4**, 799 (2008).

[55] H. Liu, H. Jiang, X. C. Xie, and Q. F. Sun, Spontaneous spin-triplet exciton condensation in ABC-stacked trilayer graphene, Phys. Rev. B **86**, 085441 (2012).

[56] Q. F. Sun and X. C. Xie, Spin-polarized $\nu = 0$ state of graphene: A spin superconductor, Phys. Rev. B **87**, 245427 (2013).

[57] Z. Q. Bao, X. C. Xie, and Q. F. Sun, Ginzburg-Landau-type theory of spin superconductivity, Nat. Commun. **4**, 2951 (2013).

[58] K. Ueda, H. Tabata, and T. Kawai, Ferromagnetism in $LaFeO_3$-$LaCrO_3$ superlattices, Science **280**, 1064 (1998).

[59] P. Yu *et al.*, Interface Ferromagnetism and Orbital Reconstruction in $BiFeO_3$-$La_{0.7}Sr_{0.3}MnO_3$ Heterostructures, Phys. Rev. Lett. **105**, 027201 (2010).

[60] S. M. Wu, S. A. Cybart, P. Yu, M. D. Rossell, J. X. Zhang, R. Ramesh, and R. C. Dynes, Reversible electric control of exchange bias in a multiferroic field-effect device, Nat. Mater. **9**, 756 (2010).

[61] C. He *et al.*, Interfacial Ferromagnetism and Exchange Bias in $CaRuO_3/CaMnO_3$ Superlattices, Phys. Rev. Lett. **109**, 197202 (2012).

[62] M. Gibert, P. Zubko, R. Scherwitzl, J. Iniguez, and J.-M. Triscone, Exchange bias in $LaNiO_3$-$LaMnO_3$ superlattices, Nat. Mater. **11**, 195 (2012).

[63] A. J. Grutter *et al.*, Interfacial Ferromagnetism in $LaNiO_3/CaMnO_3$ Superlattices, Phys. Rev. Lett. **111**, 087202 (2013).

[64] C. Du, H. Wang, F. Yang, and P. C. Hammel, Enhancement of Pure Spin Currents in Spin Pumping $Y_3Fe_5O_{12}$/Cu/metal Trilayers through Spin Conductance Matching, Phys. Rev. Applied **1**, 044004 (2014).

[65] Q. Wu, L. Shen, Z. Bai, M. Zeng, M. Yang, Z. Huang, and Y. P. Feng, Efficient Spin Injection into Graphene through a Tunnel Barrier: Overcoming the Spin-Conductance Mismatch, Phys. Rev. Applied **2**, 044008 (2014).

[66] H. Kroemer, Nobel lecture: Quasielectric fields and band offsets: Teaching electrons new tricks, Rev. Mod. Phys. **73**, 783 (2001).